



Originally published as:

Li, X., Ge, M., Dousa, J., Wickert, J. (2014): Real-time precise point positioning regional augmentation for large GPS reference networks. - *GPS Solutions*, 18, 1, p. 61-71.

DOI: <http://doi.org/10.1007/s10291-013-0310-3>

Real-time precise point positioning regional augmentation for large GPS reference networks

Xingxing Li^{a,b}, Maorong Ge^a, Jan Dousa^c, Jens Wickert^a

a. The German Research Centre for Geosciences (GFZ), Telegrafenberg, 14473 Potsdam, Germany;

lixin@gfz-potsdam.de, maor@gfz-potsdam.de, wickert@gfz-potsdam.de

b. Wuhan University, 129 Luoyu Road, 430079, Wuhan, Hubei, China;

c. Research Institute of Geodesy, Topography and Cartography, Ústecká 98, 250 66 Zdíby, Czech Republic;

Abstract: An increasing number of GNSS reference stations are installed around the world to provide real-time precise positioning services. In most of the current services, a full network solution is required for the precise determination of biases. Such a network solution is time-consuming and difficult to achieve for very large regions such as Europe or China. Therefore, we developed a multi-layer processing scheme for precise point positioning (PPP) regional augmentation to avoid processing large networks. Furthermore we use L1 and L2 raw observations and estimate atmospheric delays, which were properly constrained to the atmospheric corrections derived from the reference stations. Therefore, inaccurate representation of atmospheric delays due to temporal and/or spatial atmospheric fluctuations in the processing can be compensated. The proposed scheme of PPP regional augmentation was implemented into the operational real-time PPP service system at GFZ for validation. The real-time orbit and clock corrections, the uncalibrated phase delays and regional augmentation corrections are generated by this system. The augmentation corrections from the regional network are investigated and the positioning performance in terms of positioning accuracy and time for fixed solution is demonstrated in real-time. Our results indicate that a reliable fixing is possible after five seconds on average. The positioning accuracy is about 12, 10 and 25 mm in east, north and vertical direction, respectively.

Keywords: Real-time Precise Point Positioning; Regional Augmentation; Large Reference Network; Undifferenced Integer Ambiguity; Atmospheric Constraints

27 **1 Introduction**

28 Network-based real-time kinematic (NRTK) positioning with instantaneous ambiguity resolution (Fotopoulos and Cannon
29 2001; Landau et al. 2007) and real-time precise point positioning (PPP) (Zumberge et al. 1997; Dow et al. 2009) are currently
30 popular techniques for real-time precise positioning. In most of the current NRTK approaches, an integrated solution for all
31 reference stations is carried out in order to provide adequate atmospheric corrections needed for reliable and precise
32 positioning. The generation of such network solution, however, is usually time-consuming and difficult to achieve for large
33 regions such as Europe or China (Bisnath and Gao 2007; Ge et al. 2011). On the contrary, a reliable real-time PPP service can
34 provide precise positioning on a global scale with a worldwide reference network of about 80 stations. But in such a case, PPP
35 needs a comparatively long initialization of about 30 minutes to get centimeter-level positioning accuracy and cannot reach the
36 accuracy of NRTK even after this initial convergence time (Kouba and Héroux 2001; Wang et al. 2002). The PPP performance
37 is expected to improve in the future when more accurate pseudorange measurements will be available or observations at
38 additional carrier frequencies (Feng 2008).

39 PPP and NRTK have specific advantages and disadvantages. To make use of the first and to reduce the latter both are being
40 further developed and improved. For example, while NRTK developments lead to support undifferenced corrections to extend
41 the service coverage (Zou et al. 2012), several augmentation methods are developed to improve the performance of global PPP
42 service in specific areas by making use of regional reference networks (Wübbena et al. 2005; Li et al. 2011; Zhang et al.
43 2011a). In the methods developed by Wübbena et al. (2005) and Zhang et al. (2011a), an integrated network solution is still
44 unavoidable which is very time-consuming and seldom available for regional networks with a large number of reference
45 stations.

46 In this contribution, a multi-layer processing scheme is developed by employing PPP for regional reference stations (Li et al.
47 2011) in order to avoid processing large networks. Moreover, we use L1 and L2 raw observations in the PPP algorithm and

48 estimate atmospheric delays using proper a priori constraint, so that ambiguities in L1 and L2 can be resolved to integers
 49 directly. Consequently, corrections can be generated at the undifferenced level and broadcasted station by station, enabling the
 50 user to decide which nearby reference stations should be selected for interpolating the corrections. In this way the heavy
 51 communication burden in most of the current NRTK methods can be decreased significantly.

52 The new processing scheme for PPP regional augmentation (PPP-RA) is implemented into the GFZ real-time precise
 53 positioning service system for validation. The performance in terms of the position accuracy and the time to fixed solution is
 54 demonstrated with a large set of real-time data.

55

56 **2 The processing scheme**

57 The observation model for PPP with raw observations is introduced first. A PPP-RA (PPP Regional Augmentation) processing
 58 scheme is then proposed for efficient estimation of different corrections. The user positioning algorithm is presented in detail
 59 afterwards.

60

61 **2.1 Observation model**

62 Since the initial phases and hardware delays cannot be easily separated, we group them as uncalibrated phase delay (UPD) for
 63 receiver and satellite respectively (Blewitt 1989). Then the observation equations of undifferenced carrier phase and
 64 pseudorange can be expressed as

$$65 \quad L_{r,j}^s = \rho_{rg}^s - t^s + t_r + \lambda_j (b_{r,j} - b_j^s) + \lambda_j N_{r,j}^s - I_{r,j}^s + T_r^s + \varepsilon_{r,j}^s \quad (1)$$

$$66 \quad P_{r,j}^s = \rho_{rg}^s - t^s + t_r + c(d_{r,j} + d_j^s) + I_{r,j}^s + T_r^s + e_{r,j}^s \quad (2)$$

67 where indexes s , r and j refer to the satellite, receiver and frequency; t^s and t_r are the clock biases of satellite and
 68 receiver; $N_{r,j}^s$ is the integer ambiguity; $b_{r,j}$ and b_j^s are the receiver and satellite UPDs; λ_j is the wavelength; $d_{r,j}$ is the
 69 signal delay from the receiver antenna to the receiver signal correlator; d_j^s is the signal delay from the satellite signal

70 generator to the satellite antenna; $I_{r,j}^s$ is the slant ionospheric delay at the frequency j ; T_r^s is the slant tropospheric delay;
71 $e_{r,j}^s$ and $\varepsilon_{r,j}^s$ are the pseudorange and carrier phase measurement noise. Furthermore, ρ_g denotes the geometric distance
72 between the electronic phase centers of the satellite and receiver antennas at the signal transmission and receiving epochs. The
73 phase center offsets and variations and the station displacement due to tidal loading must be considered. Other corrections such
74 as phase wind-up or relativistic delays must be precisely applied according to the existing models.

75 The slant tropospheric delay consists of the dry and wet component. Both can be expressed by their individual zenith
76 delay and mapping function (Boehm et al. 2006). The tropospheric delay is usually corrected for its dry component with an a
77 priori model, e.g. dry Saastamoinen model while the residual part of the tropospheric delay (considered as zenith wet delay
78 Zwd_r) at the station r is estimated from the observations

$$79 \quad L_{r,j}^s = \rho_{rg}^s - t^s + t_r + \lambda_j(b_{r,j} - b_j^s) + \lambda_j N_{r,j}^s - I_{r,j}^s + Zwd_r \cdot M_r^s + \varepsilon_{r,j}^s \quad (3)$$

$$80 \quad P_{r,j}^s = \rho_{rg}^s - t^s + t_r + c(d_{r,j} + d_j^s) + I_{r,j}^s + Zwd_r \cdot M_r^s + e_{r,j}^s \quad (4)$$

81 where M_r^s is the wet mapping function.

82 For multi-frequency observations, the ionospheric delays at different frequency can be expressed as

$$83 \quad I_{r,j}^s = \lambda_j^2 / \lambda_k^2 \cdot I_{r,k}^s \quad (5)$$

84 The ionospheric delays can be eliminated by the linear combination of observations at different frequencies. Usually, the
85 ionosphere-free observation is used for PPP and for the network solution. Alternatively, the dual-frequency data can be
86 processed to also estimate the slant ionospheric delays in the raw observations (Schaffrin and Bock 1988; Odijk 2002). In order
87 to strengthen the solution, a priori knowledge of the ionospheric delays is utilized to constrain the estimated ionospheric
88 parameters. The temporal change in the slant ionospheric delay of a satellite-station pair can be represented by a stochastic
89 process that considers its temporal correlation (Bock et al. 2009; Dai et al. 2003). Ionospheric gradient parameters could be
90 used to represent the spatial character of the ionospheric delay distribution (Chen and Gao 2005). The temporal correlation,
91 spatial characteristics and ionospheric model constraints are comprehensively considered to improve the performance of

92 single-frequency PPP (Shi et al. 2012) and PPP ambiguity fixing (Li, 2012). These constraints, to be imposed on observations
 93 of a single station, can be summarized as

$$\begin{aligned}
 I_{r,t}^s - I_{r,t-1}^s &= w_t, \quad w_t \sim N(0, \sigma_{wt}^2) \\
 \nu I_r^s &= I_r^s / f_{r,IPP}^s = a_0 + a_1 dL + a_2 dL^2 + a_3 dB + a_4 dB^2, \sigma_{\nu I}^2 \\
 \tilde{I}_{r,GIM}^s &= I_r^s, \sigma_i^2
 \end{aligned} \tag{6}$$

95 where t is the current epoch and $t-1$ is the previous epoch; w_t is a zero mean white noise with variance σ_{wt}^2 ; νI_r^s is the
 96 vertical ionospheric delay; $f_{r,IPP}^s$ is the mapping function at the ionospheric pierce point (IPP); the coefficients
 97 a_i ($i = 0, 1, 2, 3, 4$) describe the trend; dL and dB are the longitude and latitude difference between the IPP and the station
 98 location, respectively.

99

100 2.2 An efficient strategy to derive corrections

101 Precise positioning service requires that all error components must be represented with certain accuracy in order that errors at
 102 the user stations can be mitigated to achieve the desired positioning accuracy. Theoretically, the integrated network solution is
 103 an ideal approach which, unfortunately is burdened by a high computational load that increases with the number of network
 104 stations. For example, it is very difficult to update satellite clock corrections every second using a network with more than 100
 105 stations. Therefore the integrated network solution is not applicable to regional augmentation of large areas. Taking the various
 106 properties of the different error sources into account, we developed a multi-layer processing strategy to avoid the
 107 time-consuming network solution for all reference stations. This strategy includes four layers that provide a) precise orbits, b)
 108 precise clocks, c) satellite UPDs, and d) ionospheric and tropospheric corrections. The network solution must be used within
 109 the first two layers for the estimation of precise satellite orbits and precise clocks. The orbits from the first layer will be fixed
 110 for the precise clock estimation in the second layer. In layers three and four the UPDs and ionospheric and tropospheric
 111 corrections are generated using PPP and utilizing orbits and clocks derived from the previous layers. The first two layers thus
 112 provide the standard products for PPP service as a base. If the capacity of layers three and four is integrated into this base, then

113 PPP with ambiguity resolution and PPP with regional augmentation can be supported for the user.

114 The precise orbit is usually determined in a batch-processing mode using about 100 globally distributed stations. Due to its
115 dynamic stability it is predicted for real-time applications. The GFZ provides an ultra-rapid product (GFU) updated every three
116 hours for real-time users. The clock corrections have to be estimated and updated much frequently (Zhang et al. 2011b) due to
117 their short-term fluctuation. The clock corrections can be estimated with the same or a similar network as used for the orbit
118 determination or with a regional network consisting at least of tens of stations. During clock estimation the satellite orbit and
119 station coordinates are held fixed or are tightly constrained while the satellite and receiver clocks, the ambiguities and the ZTD
120 parameters are estimated. Strong constraints on fixed double-differenced ambiguities would also enhance the solution and
121 improve the accuracy of the estimated clock products (Geng et al. 2012).

122 The UPDs estimates from a dense reference network are more stable and accurate than when estimated from a sparse
123 network (Geng et al. 2011; Li and Zhang 2012). With precise orbit and clock products, the UPDs can be estimated using
124 ambiguities from the PPP solution (Ge et al. 2008), which enables UPD to be estimated from much denser networks. In this
125 contribution, we also employ the raw observation equations of (3), (4), (5) and ionospheric constraints of (6) to derive the
126 UPDs on L1 and L2 frequency instead of using Melbourne-Wübbena (MW) and ionosphere-free (L3) combinations.

127 One possible solution for achieving instantaneous ambiguity-fixing is to provide precise atmospheric delay corrections as is
128 done in NRTK. Since the ionosphere and troposphere are spatially correlated with correlation reducing with distance, dense
129 reference networks with an inter-station baselines of several tens of kilometers are required for the precise representation of
130 atmospheric delays. This is also the major reason for deploying more than 300 stations in Germany and over 1000 stations in
131 China to provide NRTK services.

132 The key for a precise representation of all the biases is a successful ambiguity resolution of the regional reference network
133 (Li et al. 2011; Zou et al. 2012). With the orbit and clock products available, and using the undifferenced observations (3) and
134 (4), the relation (5), and ionospheric constraints (6), the PPP solution can be carried out station by station. For all regional

135 reference stations the coordinates can be fixed to speed up the convergence time. By applying the L1 and L2 UPD corrections
136 from layer 3, the integer ambiguity resolution can be attempted at any epoch in real-time. As soon as most of the undifferenced
137 integer (UD) ambiguities are fixed to integers, the undifferenced atmospheric corrections can be derived straightforwardly.
138 With the integer UD-ambiguities of the reference network, the corresponding undifferenced atmospheric corrections of
139 ionospheric slant delay and zenith wet delay can be derived station by station as

$$140 \quad I_{r,j}^s - Zwd_r \cdot M_r^s = \rho_{r,g}^s - L_{r,j}^s - t^s + t_r + \lambda_j (b_{r,j} - b_j^s) + \lambda_j N_{r,j}^s + \varepsilon_{r,j}^s \quad (7)$$

$$141 \quad -I_{r,j}^s - Zwd_r \cdot M_r^s = \rho_{r,g}^s - P_{r,j}^s - t^s + t_r + c(d_{r,j} + d_j^s) + e_{r,j}^s \quad (8)$$

142 This procedure is very easy to be realized even for the reference network with a large number of stations. Furthermore,
143 biases with different physical characteristics such as tropospheric and ionospheric delays can also be represented separately at
144 the server-end for possible improvement based on their own properties. Besides the significant improvement in the
145 computational efficiency, it is also of great importance that the corrections can be broadcasted station by station via NTRIP
146 (Networked Transport of RTCM via Internet Protocol, <http://igs.bkg.bund.de/ntrip>). A number of nearby reference stations can
147 be selected by a user according to the approximate coordinates and relevant station-wise atmospheric corrections can be
148 disseminated efficiently. The heavy communication burden in most of the current NRTK methods can be reduced significantly
149 in this way.

150

151 **2.3 Positioning Algorithm**

152 At the user-end, the same PPP algorithm described by (3) to (5) is utilized. Using the orbit and clock corrections only, the
153 standard PPP can be carried out. If any UPD product is also available, the PPP ambiguity fixing can be achieved on a global
154 scale based on tens of minutes of observations. Furthermore, if the precise atmospheric corrections from a regional reference
155 network are also accessible via NTRIP, the user can achieve almost instantaneous ambiguity-fixing by applying the
156 interpolated corrections for removal of atmospheric delays.

157 However, the atmospheric delays derived at each station could be biased due to an inaccurate modeling or other
158 station-dependent error since the lower-order polynomial interpolation might not be able to represent irregular spatial and
159 temporal fluctuations in small scales. This representation error could be reduced by deploying very dense reference networks.
160 In order to balance the representation accuracy and the density of reference stations, the ionospheric slant delay and
161 tropospheric zenith delay at the user stations are estimated as unknown parameters similar to the standard PPP using (3) to (5)
162 and properly constrained to the interpolated corrections. In this way, the standard PPP and augmented PPP can also be
163 integrated.

164 Assume that the selected reference stations are r_1 to r_n for interpolating corrections for user r_u . The ionospheric slant
165 delay parameter for an individual satellite s_i is constrained to the interpolated correction as

$$166 \quad I_{r_u}^{s_i} - \tilde{I}_{r_1, r_2, \dots, r_n}^{s_i} = w_I, \quad w_I \sim N(0, \sigma_{w_I}^2) \quad (9)$$

167 and the constraint for the zenith wet delay parameter is

$$168 \quad Zwd_{r_u} - \tilde{Zwd}_{r_1, r_2, \dots, r_n} = w_T, \quad w_T \sim N(0, \sigma_{w_T}^2) \quad (10)$$

169 where $I_{r_u}^{s_i}$ denotes the slant ionospheric delay from station r_u to satellite s_i ; $\tilde{I}_{r_1, r_2, \dots, r_n}^{s_i}$ is the interpolated ionospheric correction ;
170 Zwd_{r_u} denotes the zenith wet delay for station r_u , and $\tilde{Zwd}_{r_1, r_2, \dots, r_n}$ is the interpolated correction. The biases between the true
171 and the interpolated corrections w_I and w_T are zero mean white processes with variance of $\sigma_{w_I}^2$ and $\sigma_{w_T}^2$ for
172 ionospheric and tropospheric delays, respectively.

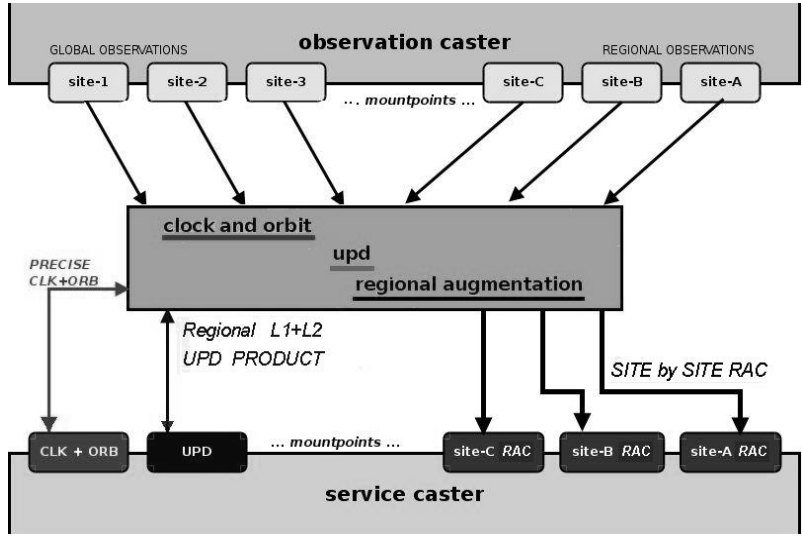
173

174 3 The PPP-RA Service System

175 The EPOS-RT software (Ge et al. 2011) has been developed in the IGS (International GNSS Service) real-time data analysis
176 center at GFZ and is used for generating real-time orbits, clocks, global ionospheric map (GIM) and UPD. Recently, the
177 software was adapted for providing regional augmentation corrections (RAC) and the corresponding client software iPPP
178 extended for using these RACs. The new system is now running operationally to provide RACs for Germany with the SAPOS

179 real-time stations.

180 The data flow at the server of the PPP-RA service is illustrated in Fig. 1. The server receives data from the observation
181 caster for both global and regional stations. The global data is employed to estimate orbits and clocks which are transmitted via
182 the service caster to users. With the orbits and clocks data, the PPP can be carried out for any reference station, so that UPD
183 can be estimated from the ambiguities of the PPP solutions. With the orbits, clocks and UPDs data being available, the integer
184 UD ambiguities on L1 and L2 frequency are fixed in PPP mode and atmospheric corrections are derived and casted to users on
185 a station basis. It should be mentioned that ambiguity resolution at the regional reference stations is very critical, as an
186 ionospheric correction can be derived only when its ambiguity is fixed. This is also shown in (7).



187

188 Fig. 1 Data flow at the server of the PPP-RA service.

189 At the user stations, the source table with the regional reference station locations should be downloaded at the beginning. At
190 least three nearby stations are selected according to the user location and the communication link is setup for continuously
191 receiving corrections. Besides the orbit, clock and UPD products used in PPP ambiguity resolution, the atmospheric
192 corrections must be interpolated and imposed as constraint on related parameters. Then the instantaneous ambiguity resolution
193 is achievable. The data flow at the user is illustrated in Fig. 2.

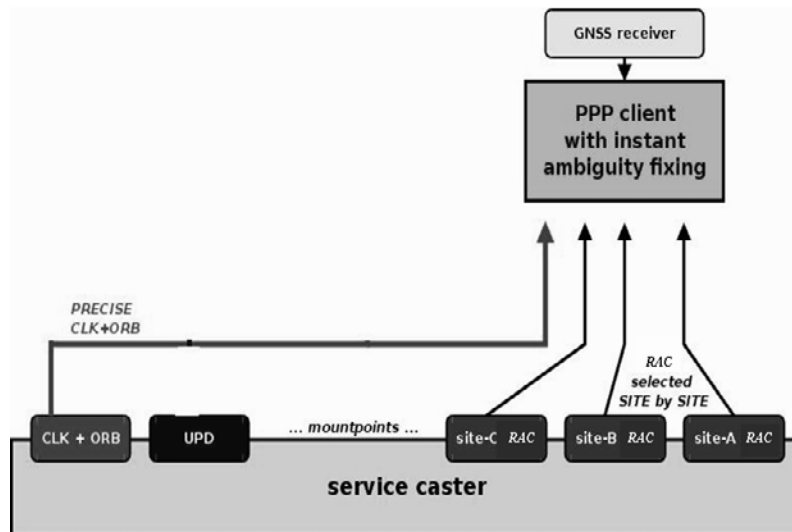


Fig. 2 Data flow at the user end for PPP-RA using regional augmentation corrections.

4 Results

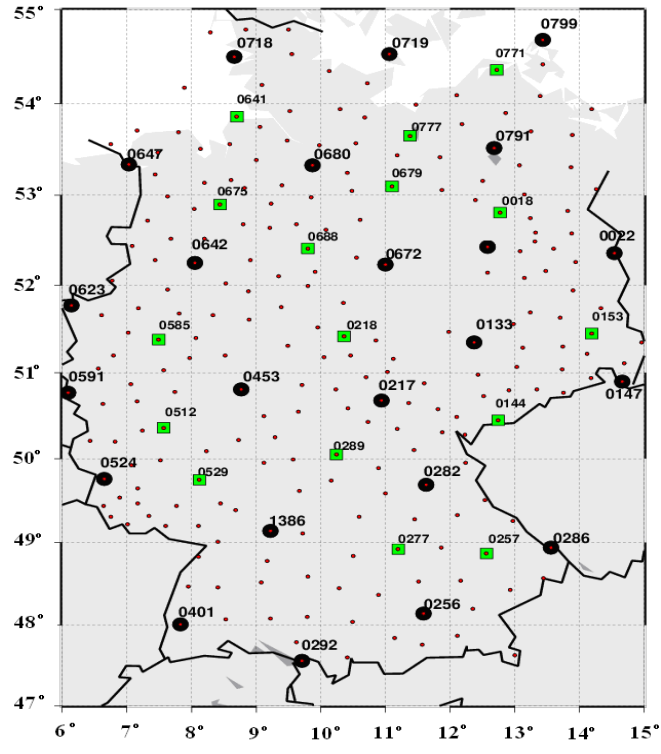
The positioning results are analyzed to validate the performance. Both, real-time positioning accuracy and time to achieve a fixed solution are evaluated using a large data set.

4.1 Data and Processing Strategy

Fig. 3 shows the distribution of the German SAPOS real-time stations. There are about 300 stations (small red dots), equipped with various types of GNSS receivers. The real-time data with 1Hz sampling rate is provided for this study. The real-time orbit and clock products are generated as described in Section 2.2. The selected regional reference stations (large black dots) are processed in PPP mode using the generated orbit and clock products, and UPDs are then estimated from these regional stations. The UD atmospheric corrections are generated on the selected regional reference stations by using the strategy introduced in Section 2.2. The corrections are broadcasted via NTRIP on the station basis.

Seventeen stations which are marked with green squares are chosen as test stations. The user positioning algorithm, as presented in Section 2.3, was applied at each test station. Three nearby reference stations are selected for interpolating corrections and a cut-off elevation angle of 10° is applied to ensure usable observations. The station coordinates are estimated epoch by epoch without any constraints between epochs. The integer ambiguity resolution is attempted epoch-wise and L1 and

211 L2 ambiguities are fixed simultaneously using the LAMBDA method (Teunissen 1995). The ratio between the minimum and
212 the second minimum quadratic form of residuals is applied to decide about the success of fixing the integer ambiguity
213 candidate while the threshold for the ratio test is set to three as usual.

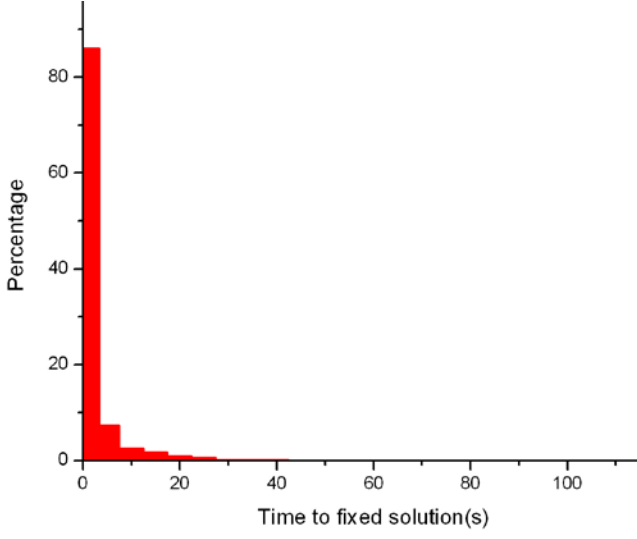


214
215 Fig. 3 Distribution of real-time stations of the SAPOS network used for this study. Each small red dot indicates a station. Large
216 black dots indicate the selected regional reference stations and the large squares refer to for user stations.

217
218 **4.2 PPP-RA Performance**

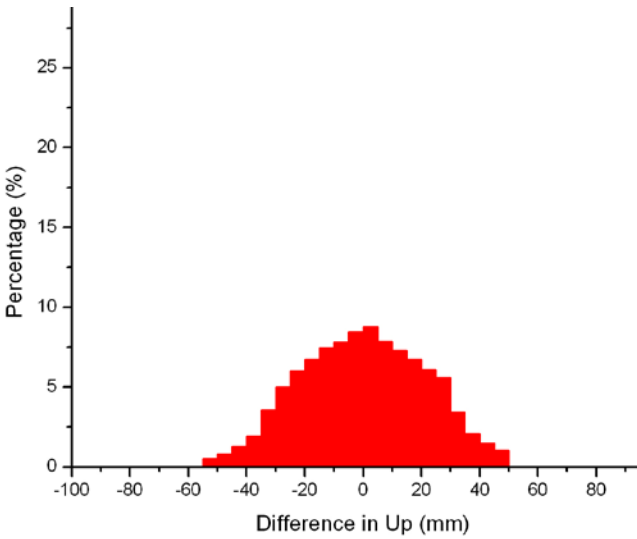
219 For the selected user stations, the estimator is restarted every minute to obtain the statistics on the time for ambiguity-fixing
220 and the position accuracy of the fixed solution. The statistical results of GPS week 1675 are shown in Figs. 4 to 6. Fig. 4 shows
221 the statistics of the observation time needed for successful ambiguity fixing. For about 87% of the solution the ambiguity can
222 be fixed with just one epoch of data. On average, data of five seconds are needed for a reliable ambiguity-fixing. We also
223 notice that there are few solutions where ambiguities cannot be fixed within the predefined restarting time of one minute.
224 Further investigation should be carried out for possible improvement.

225 As soon as the integer ambiguities have been successfully fixed, the coordinates at the epoch are used to assess the
226 positioning accuracy of the PPP-RA service. The fixed solutions are compared with the precise coordinates from
227 post-processed daily solutions. Fig. 5 shows the distribution of position differences in up direction. The vertical component has
228 a RMS of 25 mm. Fig. 6 shows the distribution of position differences in horizontal direction. The RMS of east and north
229 components are 12 mm and 10 mm respectively.



230
231

Fig. 4 Observing time needed for ambiguity-fixing



232
233
234

Fig. 5 Distribution of position errors in the vertical component.

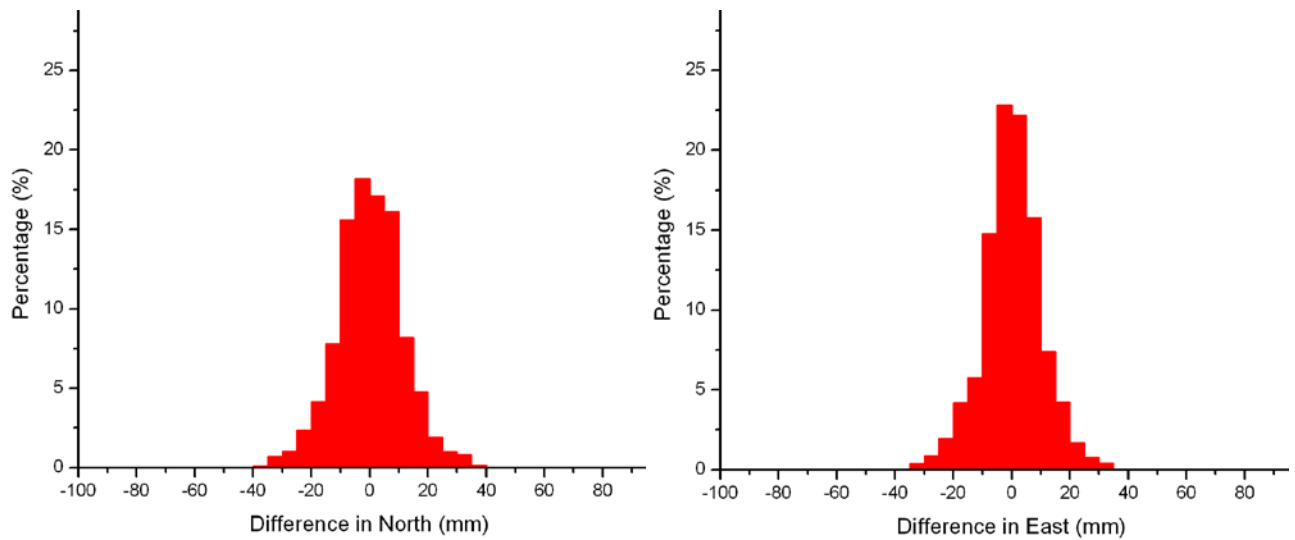
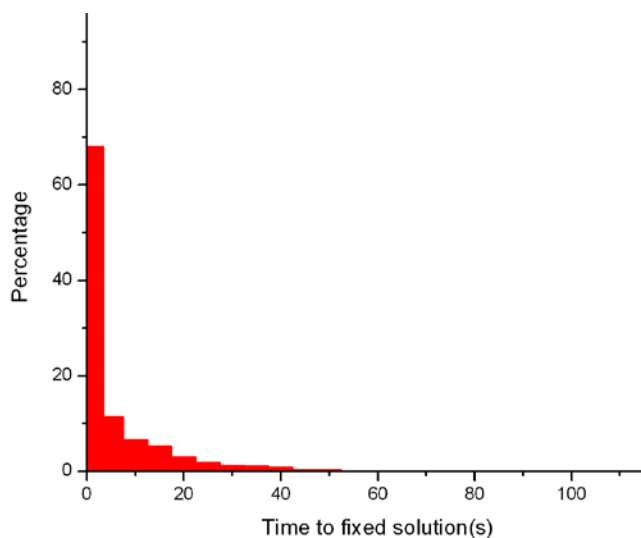


Fig. 6 Distribution of position errors in the horizontal components.

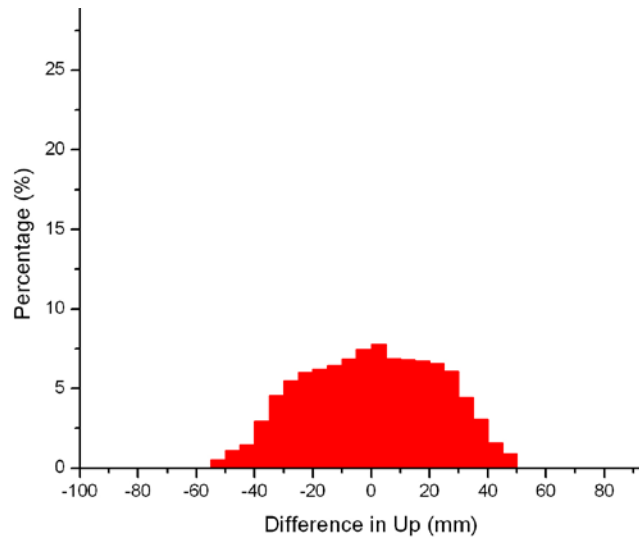
For validating the improvement of the PPP algorithm using raw observations, the PPP-RA scheme by Li et al. (2011), in which user observations are corrected directly with atmospheric corrections and wide-lane/ionosphere-free observations are employed, is also carried out in parallel. The corresponding results are shown in Figs. 7 to 9. Fig. 7 shows the statistics of observation time needed for successful ambiguity fixing. For about 68% of the solutions the ambiguity can be fixed with one epoch of data. On average, data of ten seconds are needed for a reliable ambiguity-fixing. Fig. 8 shows the distribution of position differences in the up direction. The vertical component has a RMS of about 30 mm. The RMS of east and north components (Fig. 9) are 15 and 12 mm, respectively. These results confirm that the new PPP algorithm significantly improves the ambiguity fixing performance and positioning accuracy.



246

Fig. 7 Observing time needed for ambiguity-fixing.

247

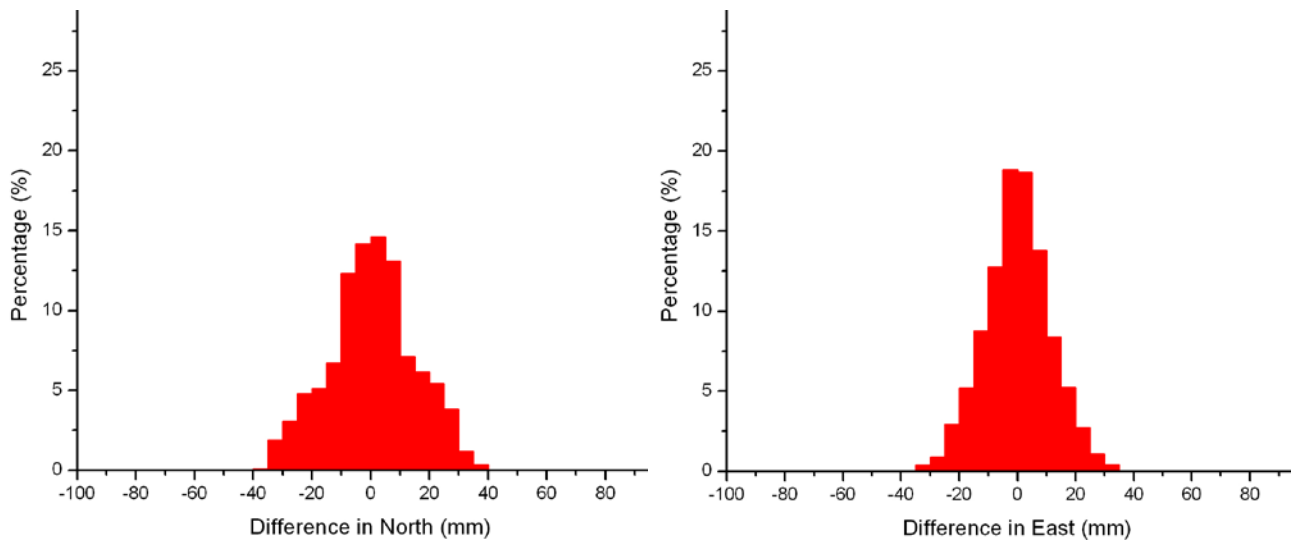


248

249

Fig. 8 Distribution of the position errors in the vertical component.

250

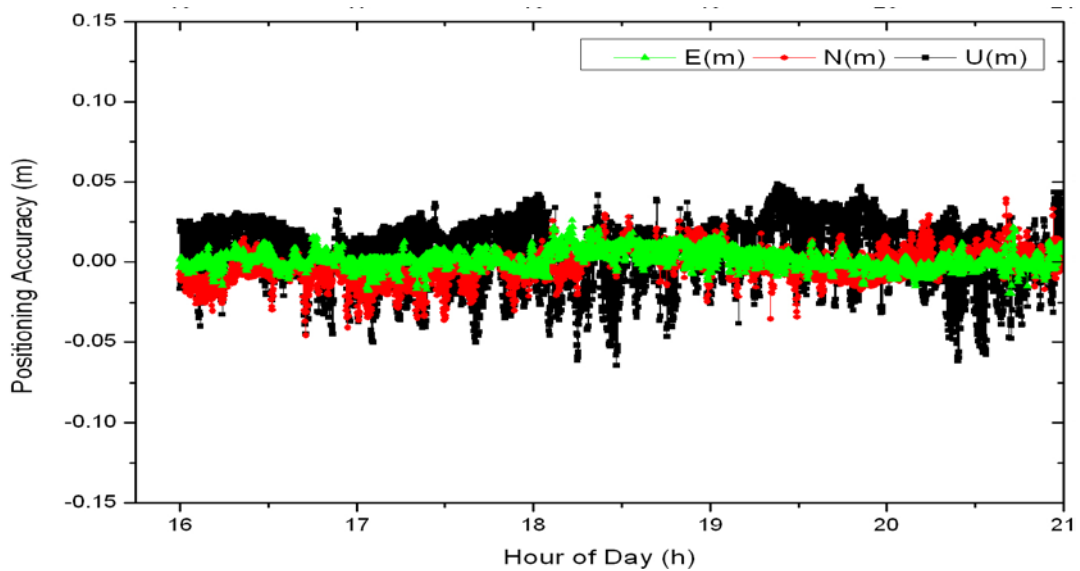


251

252

Fig. 9 Distribution of the position errors in the horizontal components.

253



254

255

Fig. 10 Positioning errors at the station 0675 on DOY 43, 2012

256

257

258

An example for the position differences of fixed kinematic PPP solution and post-processed daily solution for the SAPOS station 0675 is given in Fig. 10. This figure indicates that a position accuracy of a few centimeters is achievable using PPP with regional augmentation corrections.

259

4.3 Investigation on corrections

260

261

To better understand the level of improvement, reached by the application of the new strategy, we selected stations 0642, 0647, 0680 and 0675. The UD corrections and the interpolated values were derived and analyzed in detail.

262

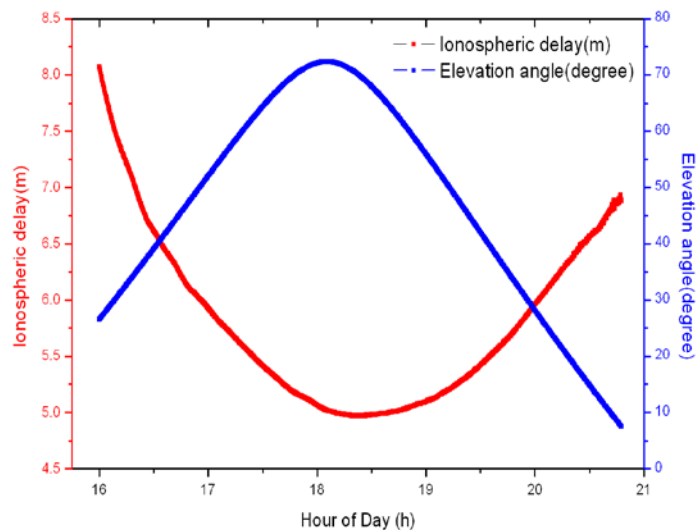
263

264

The estimated UD ionospheric delays and the corresponding elevation angles of GPS satellite PRN15 are illustrated as an example in Fig. 11 for one continuous arc from 16:00 to 21:00 on February 12, 2012 (DOY 043). One can see the temporal correlation of the ionospheric delay and the strong correlation between elevation angles and ionospheric delays. The zenith wet

265

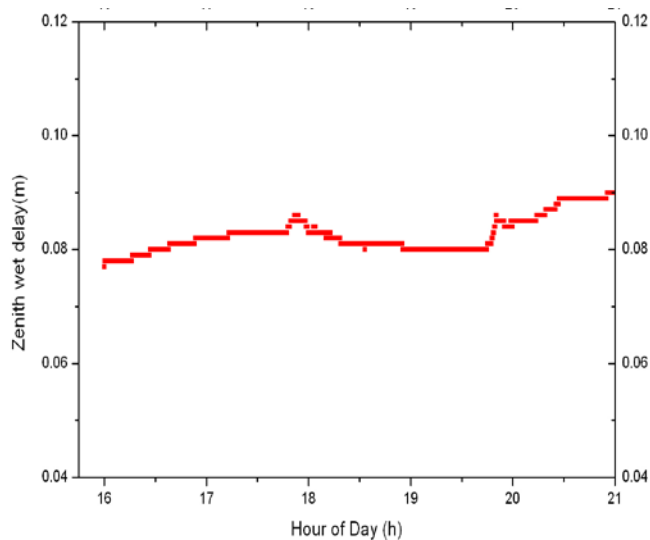
delays of the SAPOS station 0642 are shown in Fig. 12.



266

267

Fig. 11 Ionospheric delays and elevations for satellite PRN15 at station 0642 during 16:00 to 21:00



268

269

Fig. 12 Zenith wet delays at station 0642 from 16:00 to 21:00

270

271

Typical uncalibrated phase delays of GPS satellite PRN15 on L1 and L2 frequencies are shown in Fig. 13 while the

272

corresponding UPDs of wide-lane (WL) and narrow-lane (NL) combinations are shown in Fig. 14. We can observe that the

273

real-time UPDs are stable enough for a few hours, and the WL UPDs are stable over even a much longer interval.

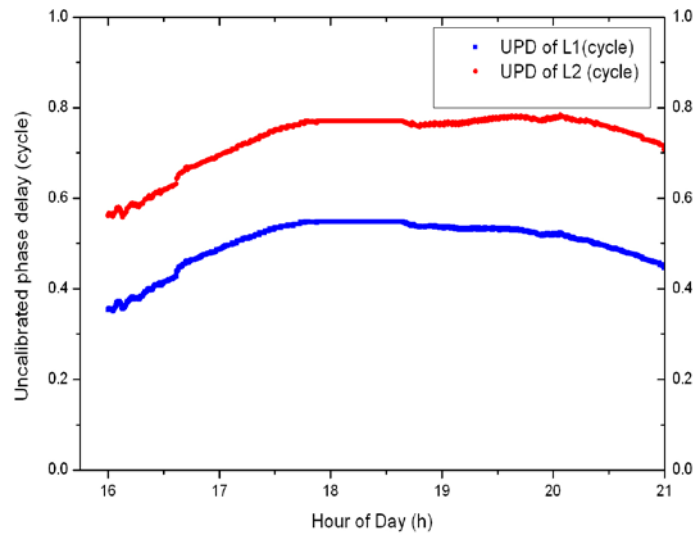


Fig. 13 Uncalibrated phase delays of satellite PRN15 on L1 and L2 frequencies

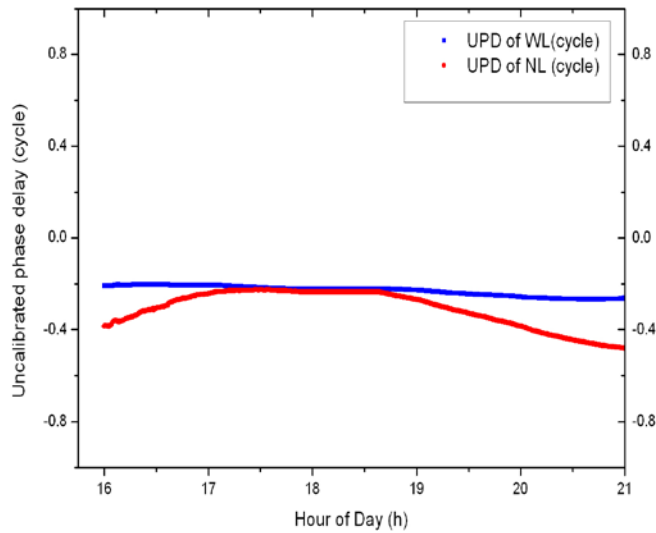
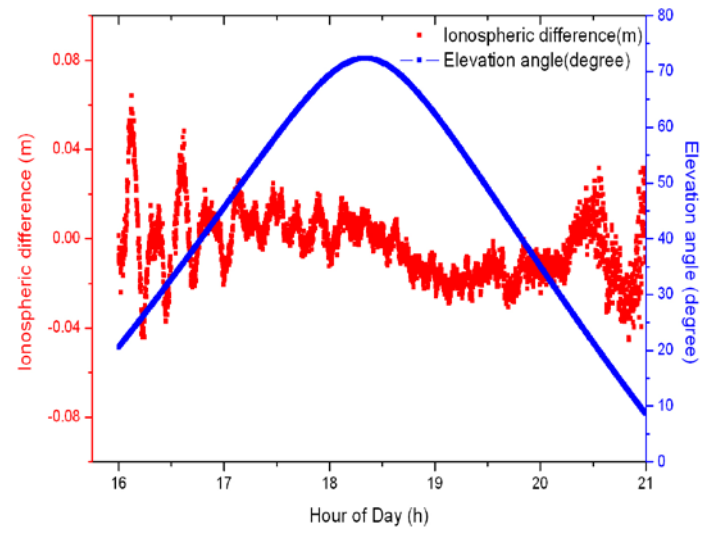


Fig. 14 Uncalibrated phase delays of satellite PRN15 on WL and NL combinations

With the UD atmospheric delays retrieved at the augmentation stations 0642, 0647 and 0680, the atmospheric delays of user station 0675 are interpolated epoch by epoch with the linear combination method. The resulting interpolations are compared with the retrieved values as was done similarly at the reference stations in order to assess the accuracy of the interpolation. Fig. 15 shows the differences for satellite PRN15, the differences are seen to be generally smaller than 5 cm with RMS of 2 cm. Tropospheric interpolation errors are shown in Fig. 16. Since the accuracy of zenith wet delay interpolation is better than 1 cm, the corrections are accurate enough for rapid ambiguity fixing.

285

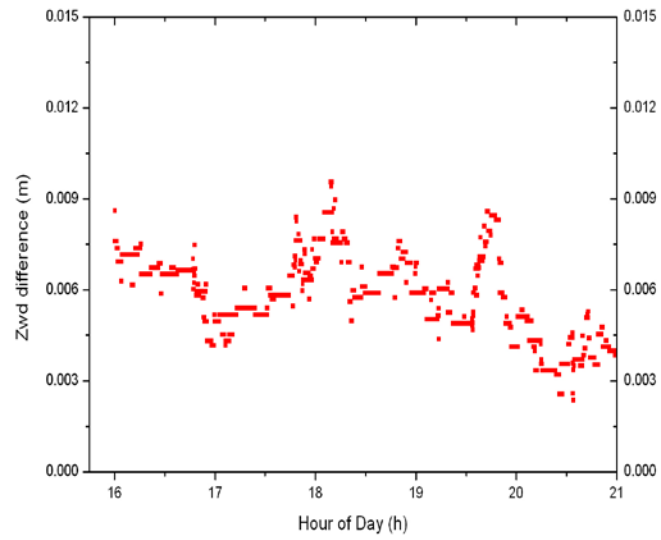


286

287

Fig. 15 Ionospheric modeling errors and elevation angles of PRN15 at station 0675

288



289

290

Fig. 16 ZWD modeling errors at station 0675

291 5 Conclusions

292 A multi-layer strategy for precise GNSS data processing was developed and introduced in order to realize PPP augmentation
 293 with a large number of reference stations. The generation of orbits and clocks as incorporated in the current real-time PPP
 294 system at GFZ are included as two basic layers. This makes it possible that PPP can be utilized for any station, including the
 295 regional reference stations, in the other two layers that pertain to the estimation of UPDs and regional augmentation corrections.

296 At each reference station, the integer ambiguity on L1 and L2 frequency are fixed in PPP mode by using raw observations.
297 Once most of the UD-ambiguities of the reference stations are resolved, the corresponding undifferenced atmospheric
298 corrections can be derived and broadcasted station by station to users.

299 The atmospheric delays, derived at each station could be biased due to inaccurate modeling or station-dependent error, and
300 the lower-order polynomial interpolation might not be able to represent irregular spatial and temporal fluctuations of small
301 scales. Therefore, we use L1 and L2 raw observations with atmospheric delay parameters which are constrained properly to the
302 interpolated atmospheric corrections. A proper constraint, which matches the accuracy of corrections, can compensate the
303 remaining systematic biases caused by large inter-station distances.

304 The new PPP-RA scheme is implemented into the EPOS-RT software and is running operationally at GFZ to demonstrate
305 the positioning performance in accuracy and time for fixed solutions. The statistics show that ambiguities can be fixed with
306 just one epoch of data in about 87% of the cases, and five seconds are needed on average for reliable ambiguity-fixing. After
307 ambiguity fixing, the RMS of the PPP position differences, compared to the daily static solution, is about 12, 10 and 25 mm in
308 east, north and vertical components, respectively.

309

310 **Acknowledgements**

311 We thank the International GNSS Service and SAPOS Germany with its central office for providing real-time data for this
312 study. The authors would also like to give their special thanks to Dr. Jake Griffiths and an anonymous reviewer. Their valuable
313 comments and suggestions improved the manuscript greatly.

314

315 **6 References**

316 Bisnath S, Gao Y (2007) Current state of precise point positioning and future prospects and limitations. Observing our
317 changing Earth, International Association of Geodesy Symposia 133, Springer-Verlag Berlin Heidelberg, pp. 615–623
318 Blewitt G (1989) Carrier phase ambiguity resolution for the global positioning system applied to geodetic baselines up to 2,000

319 km. *J Geophys Res* 94(B8):10187-10203. doi:10.1029/97JB03534

320 Bock H, Jäggi A, Dach R, Schaer S (2009) GPS single-frequency orbit determination for low Earth orbiting satellites. *Adv in*
321 *Space Res*, 43(5): 783-791

322 Boehm J, Niell A, Tregoning P, Schuh H (2006) Global Mapping Function (GMF): A new empirical mapping function based
323 on numerical weather model data. *Geophys. Res. Lett.* 33, L7304, doi: 10.1029/2005GL025546

324 Chen K, Gao Y (2005) Real-Time Precise Point Positioning Using Single Frequency Data. *Proceedings of ION GNSS-2005*,
325 September 2005, Long Beach, CA, pp.1514-1523

326 Dai L, Wang J, Rizos C (2003) Predicting atmospheric biases for real-time ambiguity resolution in GPS/GLONASS reference
327 station networks. *J Geod.* 76(11/12), 617-628

328 Dow JM, Neilan RE, and Rizos C (2009) The International GNSS Service in a changing landscape of Global Navigation
329 Satellite Systems, *J Geod.*, 83(3/4):191-198, DOI: 10.1007/s00190-008-0300-3

330 Feng Y (2008) GNSS three carrier ambiguity resolution using ionosphere-reduced virtual signals. *J Geod.*, 82(12):847-862

331 Fotopoulos G, Cannon M (2001) An overview of multi-reference station methods for cm-level positioning. *GPS Solutions*,
332 4(3), 1-10

333 Ge M, Gendt G, Rothacher M, Shi C, Liu J (2008) Resolution of GPS carrier-phase ambiguities in precise point
334 positioning (PPP) with daily observations. *J Geod* 82(7):389-399. doi:10.1007/s00190-007-0187-4

335 Ge M, Dousa J, Li X, Ramatschi M, Wickert J (2011), A Novel Real-Time Precise Positioning Service System: Global Precise
336 Point Positioning with Regional Augmentation, in: *Proceedings of the 3rd Int. Colloquium - Galileo Science*, 31 August -
337 2 September 2011, Copenhagen, Denmark

338 Geng J, Teferle F, Meng X, and Dodson A (2011) Towards PPP-RTK: Ambiguity resolution in real-time precise point
339 positioning. *Adv in Space Res*, 47 (10) 1664-1673

340 Geng J, Shi C, Ge M, Dodson AH, Lou Y, Zhao Q, Liu J (2012), Improving the estimation of fractional-cycle biases for
341 ambiguity resolution in precise point positioning, *J. Geod.* , 86(8):579-589, doi:10.1007/s00190-011-0537-0

342 Kouba J, Héroux P (2001) Precise point positioning using IGS orbit and clock products. *GPS Solutions* 5(2):12-28.
343 doi:10.1007/PL00012883

344 Landau H, X Chen, S Klose, R Leandro, U Vollath (2007) Trimble's RTK and DGPS Solutions in Comparison with Precise

345 Point Positioning, Observing our Changing Earth, International Association of Geodesy Symposia 133, Proceedings of the
346 2007 IAG General Assembly, Perugia, Italy, July 2–13, pp. 709-718

347 Li X, Zhang X, Ge M (2011) Regional reference network augmented precise point positioning for instantaneous ambiguity
348 resolution. *J. Geod.*, 85(3):151-158, Doi: 10.1007/s00190-010-0424-0

349 Li X, Zhang X (2012) Improving the Estimation of Uncalibrated Fractional Phase Offsets for PPP Ambiguity Resolution. *J.*
350 *Navig.* 65(3):513-529 doi:10.1017/S0373463312000112

351 Li X (2012) Improving Real-time PPP Ambiguity Resolution with Ionospheric Characteristic Consideration. Proc. of ION
352 GNSS-12, Institute of Navigation, Nashville, Tennessee, September,17-21

353 Odijk D (2002) Fast precise GPS positioning in the presence of ionospheric delays. Netherlands Geodetic Commission,
354 Publications on Geodesy, Vol 52, pp. 242

355 Schaffrin B, Bock Y (1988) A unified scheme for processing GPS dual-band phase observations. *Bull. Geod.* 62(2):142-160

356 Shi C, Gu S, Lou Y, Ge M (2012) An improved approach to model ionospheric delays for single-frequency Precise Point
357 Positioning. *Adv in Space Res*, 49(12):1698–1708

358 Teunissen PJG (1995) The least squares ambiguity decorrelation adjustment: a method for fast GPS integer estimation. *J.*
359 *Geod.*, 70(1/2): 65-82

360 Wang J, Satirapod C, Rizos C (2002) Stochastic assessment of GPS carrier phase measurements for precise static relative
361 positioning. *J. Geod.*, 76(2):95-104

362 Wübbena G, Schmitz M., Bagge A (2005) PPP-RTK: precise point positioning using state-space representation in RTK
363 network, Proc. of ION GNSS-05, Institute of Navigation, Inc., Fairfax, USA, pp. 2584–2594

364 Zhang B, Teunissen PJG, Odijk D (2011a) A novel undifferenced PPP-RTK concept. *J. Navig.* , 64(S1):S180-S191
365 doi:10.1017/S0373463311000361

366 Zhang X, Li X, Guo F (2011b) Satellite Clock Estimation at 1 Hz for Realtime Kinematic PPP applications. *GPS Solutions*
367 15(4): 315-324, doi: 10.1007/s10291-010-0191-7

368 Zou X, Ge M, Tang W, Shi C, Liu J (2012) URTK: undifferenced network RTK positioning. *GPS Solutions (Online First)*, doi:
369 10.1007/s10291-012-0277-5

370 Zumbeke JF, Heflin MB, Jefferson DC, Watkins MM, Webb FH (1997) Precise point positioning for the efficient and robust

371 analysis of GPS data from large networks. J Geophys Res 102(B3):5005-5017. doi:10.1029/96JB03860

372

373 **Biography (about 50 words per author)**

374 Mr. Xingxing Li is a Ph.D. student at the Department of Geodesy and Remote Sensing of the German Research Centre for
375 Geosciences (GFZ). He holds a B.S. degree in Geodesy and Geomatics from Wuhan University in China. His current research
376 focuses on the development of real-time GNSS precise positioning techniques.

377 Dr. Maorong Ge received his PhD in Geodesy at Wuhan University, Wuhan, China. He is now a senior scientist at the German
378 Research Center for Geosciences (GFZ Potsdam). He was technically in charge of the IGS Analysis Center and is now leading
379 the development of the GNSS real-time software EPOS-RT at GFZ. His research interests are GNSS algorithms and software
380 development.

381 Jan Douša received his PhD in geodesy from the TU Prague in 1999. Since 2000 he has been at the Geodetic Observatory
382 Pecný (GOP) of the Research Institute of Geodesy, Topography and Cartography for precise GNSS applications including
383 strategies and software developments. He is responsible for GOP analytical contributions to the IGS (precise ultra-rapid orbits),
384 the EUREF (European reference frame), and the E-GVAP project (global and European near real-time zenith tropospheric
385 delay estimations) .

386 Dr. Jens Wickert graduated in physics from the Technical University Dresden and obtained his doctor degree in 2002 from the
387 Karl-Franzens-University Graz in Geophysics/Meteorology. He worked in atmospheric research for several German Research
388 Institutes before starting in GNSS science in 1996. He is deputy head of the section “GPS/Galileo Earth Observation” at the
389 German Research Center for Geosciences GFZ at Potsdam. Dr. Wickert is involved in many national and international satellite
390 missions and research projects.